# Quantitative Evaluation of Standing Stabilization Using Stiff and Compliant Actuators

Jorhabib Eljaik*, Zhibin Li†, Marco Randazzo‡, Alberto Parmiggiani‡,
Giorgio Metta ‡, Nikos Tsagarakis† and Francesco Nori*
*Department of Robotics, Brain and Cognitive Sciences
Email: {jorhabib.eljaik},{francesco.nori}@iit.it
†Department of Advanced Robotics
Email: {zhibin.li},{nikos.tsagarakis}@iit.it
‡iCub Facility
Email: {marco.randazzo},{alberto.parmiggiani},{giorgio.metta}@iit.it
All departments are from Istituto Italiano di Tecnologia. Via Morego 30, 16163 Genova, Italy

***Abstract*—In this paper we evaluate the benefits of series elastic actuation in performing a balancing task on a humanoid robot. By having the possibility to replace the type of transmission at the ankles level, it was possible to repeat the very same experiment in two different conditions: (1) Using series elastic actuators (SEA); (2) Replacing the elastic elements with rigid transmissions. The experiments consisted in perturbing a balanced posture with an impulsive force. Perturbations were applied in two different scenarios: hitting the robot on the upper body and at the support platform, thus acting above and under the actuated joint. The applied perturbations were controlled to be repeatable and the static stiffness of the rigid and elastic actuators were tuned to match. With these assumptions, static responses were the same in the two conditions; differences appeared only during the dynamic response and are motivated by different proportions between active and passive stiffness. In both scenarios, results show that series elasticity simplifies the role of the balancing controller by low pass filtering the dynamics of the zero moment point, consistently observing a more stable balance recovery with SEA through all the experiments.**

## I. Introduction

Humanoid robots are designed to have an anthropomorphic structure with trunk, arms and legs. While bipedal walking solves the problem of mobility allowing humanoids to ambulate, it is also interesting to understand how legs could help arms' operation. For example, during the execution of manipulation tasks of the upper limbs, the balancing capability becomes essential in order to stabilize the robot. Stability and soft interactions are commonly the desired safety features for the coexistence of robots and humans in the same workspace, and also main requirements for stable manipulation in standing humanoids.

One effective approach for upright balance is the introduction of passive compliance. This characteristic ensures softer interaction during contacts to prevent large collision forces, and it also naturally raises up the force and torque required to recover to equilibrium as deformation accumulates. Passive compliance is commonly introduced to guarantee stability because it attenuates the excessive energy exchange during possible collisions while the robot interacts with the environment. For robots with torque controlled joints, such as the Sarcos robot [6] [19] and the DLR robots [13] [14], this is realized by controlling the virtual impedance, namely the virtual spring and dampers at the center of mass (COM) followed by computing the desired joint torques in order to generate suitable contact forces to achieve such compliant and damped effect.

However, considering that torque controlled actuators are less readily available for various technical reasons, it becomes also interesting to investigate the implementation of a compliant behavior using position controlled actuators. The work in [12] [11] presents a way to modulate positional references of the robot's COM based on the center of pressure (COP) feedback coming from the feet. The same control framework was applied to both stiff and series elastic joints. It was found that by trading off the control bandwidth introducing elasticity between the gearbox shaft and the output link, the system gains instantaneous shock absorption since controlled compliance with stiff actuators presents inevitable delays.

Most humanoid platforms developed in the past focus on mobility. The Honda ASIMO[5], HUBO [15], and HRP4-C[9] were developed for bipedal walking. The Sony QRIO [8] and the Aldebaran NAO [3] were the small scale humanoids for the purposes of entertainment, research and education. These robots share the same actuation type, namely, stiff position-controlled joints. While they provide precise position tracking, the adaptability to physical interaction and robustness to accidental collisions are limited.

Although the effect of collisions in real world applications for humanoids can be partly addressed by actively controlling the level of compliance, there is still the necessity of safety enhancement at the hardware level. Incorporating compliant materials into the actuation system, such as the series elastic actuators (SEA) [17], is usually thought to be useful. Unlike the compliance produced by the controller, physical compliance can counteract impacts in shorter time. This serves as motivation to develop humanoid robots with SEA in all or a subset of their principal joints. The first robot to use SEA was the Cog robot developed by Brooks et al. [1], followed by the M2V2 robot by Pratt and Krupp [18] and the DOMO

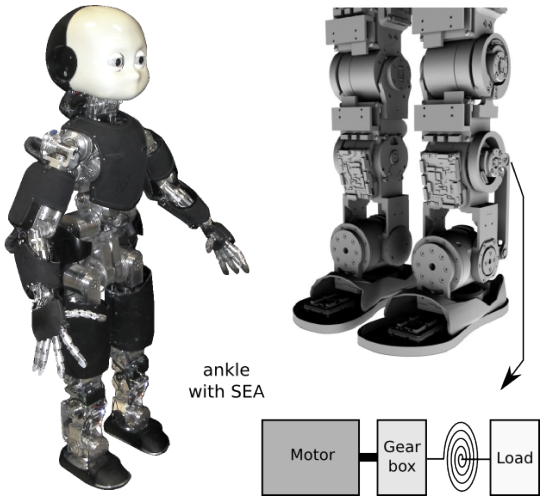


Fig. 1. Picture of iCub 2.0 with a 3D view of its legs and an ilustrative scheme of a SEA and its location on the robot. Legs 3D render by Laura Taverna.

upper body by Edsinger and Weber [2] from Meka Robotics. A similar design is employed for the BioRob arm[10]. The compact size SEA developed by Tsagarakis et al. [21] was integrated into the COMAN humanoid [22]. The DLR hand arm system [4] exploits floating spring joints (FSJ) [23].

The experimental testbed in this paper is the iCub 2.0 humanoid platform which incorporates some features of COMAN [22]. In this version, the knee and ankle joints of iCub have SEA with high resolution position sensing for accurate torque measurement. Moreover, the design of this SEA allows the locking of the actuator to turn it into a standard stiff one. The stabilization controller described in [12] has been employed for upright balance. The goal of this paper is therefore to quantitatively compare the performance of the balance controller using SEA with the exact same platform without passive elasticity. A collision test is designed using a falling mass to examine the robot's balance performance.

This paper is organized as follows. Section II describes the mechanical design and specifications of the SEA unit. Section III briefly explains the stabilization control method while Section IV shows the experimental setup and data analysis. Conclusions and future work are found in Section IV.

## II. Design of the SEA elastic module

The SEA module employed was developed from a similar design sub-assembly of the COMAN robot. A suitable value for the torsional stiffness of the elastic module for tasks such as walking and balancing, was determined in experiments with the COMAN humanoid robot. The optimal value was determined to be in the range from 300 to $350[Nm/rad]$. Being the maximum leg actuator torque in the ballpark of $40[Nm]$, the corresponding passive angular deflection of the SEA which permits the delivery of the peak torque within the elastic deflection range is in the order of of $0.1333[rad]$.

The elastic module of the COMAN robot however could not achieve such torsional stiffness values. Walking experiments showed that the elastic deflection limit was reached at $\approx 50\%$ the maximum torque, therefore reducing the advantages of the integration of SEA modules. It was then considered possible alternative designs of the elastic module.

The SEA module of COMAN comprises three pairs of opposing helical springs [21], which were thought to be substituted with other types. Possible options were: helical, disk, volute and leaf springs. The appropriate type of spring needed to comply with keeping the size of the elastic module as close as possible to the original design. However none of these alternatives allowed to obtain the desired torsional rigidity. Indeed the selection of the spring presents a very delicate trade-off problem between the spring stiffness, its maximum deflection before yielding (that required bigger springs) and the available space (that constrained the size of the springs).

We finally considered a "curved beam" spring, dubbed "C-spring", because of its shape, somewhat similar to the Robonaut torsional spring [7].

A preliminary calculation of the deflection of a curved beam, was based on the classical equations of linear elasticity [20]. We employed Castigliano's theorem to derive a closed form analytical equation that relates the spring geometry to its torsional stiffness. We then conducted a finite element analysis (FEA) on the "C-spring" to verify its torsional stiffness value: the displacement under load closely matched the analytical predictions and the maximum Von Mises equivalent stresses was confirmed to be well below the elastic limit of the material. The interested reader is referred to [16] for additional details regarding the mechatronic design of the SEA module.

The proposed elastic element design has the advantage of providing great design flexibility if compared to other implementations based on helical springs. Indeed the dimensioning of the elastic element can be effectively performed to match a wide range of desired stiffness levels.

### A. Elastic element embodiment

The final embodiment of the subsystem is represented in Fig.2. Two magnetic encoders (an absolute and a high resolution relative one) were integrated in the module for deriving joint torque measurements.

Fig.2(a) shows a cross section drawing of the elastic module. Fig.2(b) shows in detail how the module is assembled; the figure also shows the protrusions in the "motor output" part that constitute the hardware limits for the spring.

It was decided to construct the elastic element in X5CrNiCuNb16-4[1] stainless steel because of its ultimate tensile strength (UTS) of $1100[MPa]$.

The shape we adopted for the elastic element also provides a very convenient way for changing the connecting element. If a rigid joint is required (as in the case of the present study) it is sufficient to replace the SEA spring with a rigid element as shown in Fig.3.

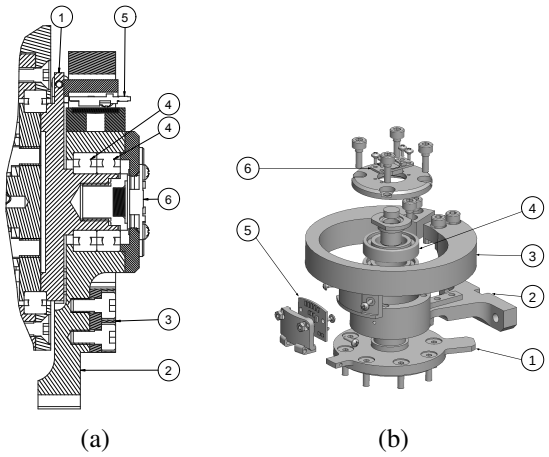


Fig. 2. SEA module. The figure shows a cross section drawing (a), and a CAD view (b) of the "C-spring" SEA module. The labelled sub-components are: the motor output part (1), the SEA module output part (2), the "C-spring" (3), the two ball bearings (4), the high resolution relative encoder based on the AS5311 IC (5), and the absolute magnetic encoder based on the AS5040 IC (6).

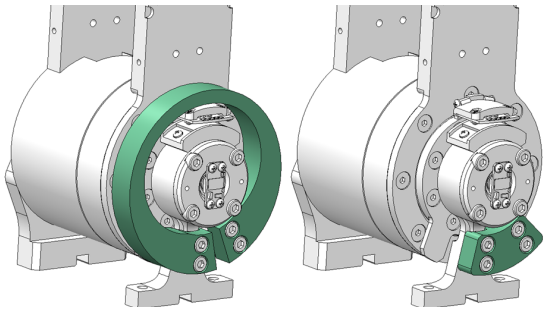


Fig. 3. Substitution of the element connecting the motor output and the joint output allows obtaining a SEA joint (a) and a rigid joint (b) on the same setup.

## III. Standing Stabilization Control

Fig. 4(a) shows a simplified model of the robot, represented by an inverted pendulum connected to a foot with a torsional spring of stiffness $k_s$ and this can vary according to the mechanical configuration (compliant or stiff transmission). The parameter $k$ is the resultant stiffness observed from the COM behavior which is determined by both the mechanism and the active controller. In Fig. 4(a) and 4(b) the real and referential COM are marked black and red respectively. Fig. 4(b) depicts how by changing the COM reference, the resultant stiffness observed by an external load can be controlled. In this case, the forward perturbation causes the COP to move forward, the robot would behave in a more compliant manner if the COM reference could be modulated forward accordingly. Contrarily, if the COM reference moves in the opposite direction of the COP motion, the observed stiffness $k$ would be higher than the

[1]See material datasheet http://www.aksteel.com/pdf/markets_products/stainless/precipitation/17-4_PH_Data_Sheet.pdf

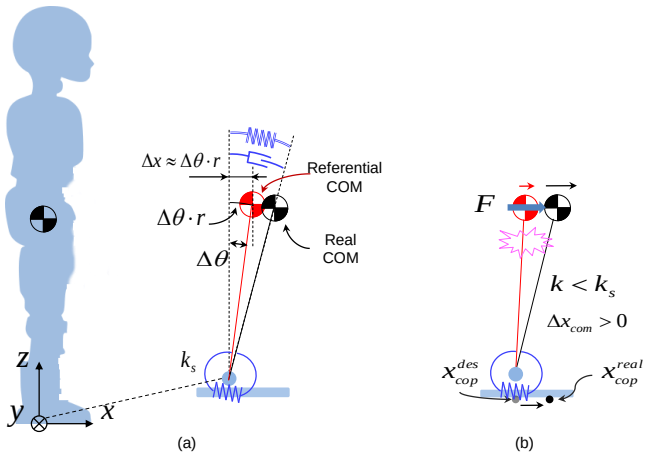


Fig. 4. Compliance control by regulating the COM reference

real stiffness $k_s$, which is not preferred for stabilization since more energy is injected into the system causing instability.

To stabilize the standing posture, a compliance control scheme is applied based on the positional modification of the COM using the COP feedback. This is analogous to the admittance control technique whereby the position perturbations computed from the applied forces are superimposed to the reference position of a stiff position controller in order to emulate a compliant behavior.

Let $\theta^{des}$ and $x_{cop}^{des}$ be the desired angular position of the ankle and the COP at the static equilibrium respectively, $\Delta x_{cop} = x_{cop}^{real} - x_{cop}^{des}$ the input of the controller and $\Delta\theta$ its output. The compliance control of the ankle joint is expressed in a simple PID form as

$$\Delta\theta(i) = k_p \Delta x_{cop}(i) - k_d \Delta \dot{x}_{cop}(i) - k_i \sum_{j=N}^{0} \Delta \tilde{x}_{cop}(i-j)\Delta t, \tag{1}$$

where $k_p > 0$, $k_d > 0$, and $k_i > 0$ are the proportional, derivative, and integral gains respectively, and $\Delta t$ is the sampling time.

The proportional gain $k_p$ determines how much the reference COM should be modified in the same direction of the COP in order to modulate the compliance of the system to external disturbances. Hence, the bigger $k_p$ is, the more compliant the robot becomes. The gain $k_d$ plays the role of a damper on the referenced COM motion. Considering that the compliant behavior will introduce steady state error, the integral term is included for removing the static offset of the COP. $\tilde{x}_{cop}$ denotes the filtered COP signal for the integral term. Integral windup is solved by using a limited time window with $N$ samples in addition to setting an upper and lower limit.

## IV. Experiments and Comparison

In this section the balancing performance of the robot is evaluated through two different experiments: a direct impact on the robot's body and an impact on a mobile platform on which the robot stands, with the aim of perturbing the

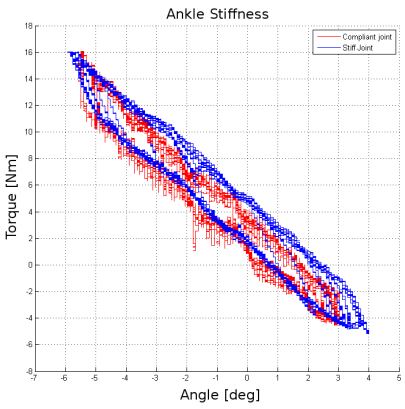


Fig. 5. The overall (active+passive) stiffness at the ankle joint. The gains of the balance controller were experimentally tuned in order to achieve the same equivalent stiffness both with stiff and series elastic joints (stiff joint: $kp = 0.4$, $kd = 0.005$; elastic joint: $kp = 0.3$, $kd = 0.08$).

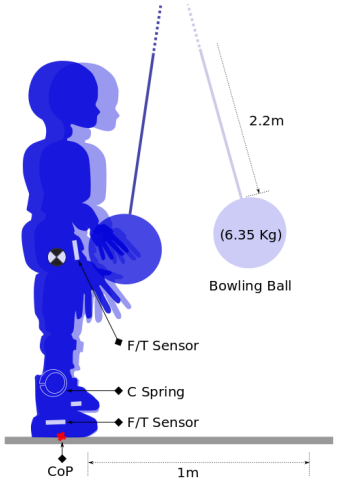


Fig. 6. A sketch of the first experimental scenario: impact on the robot body.

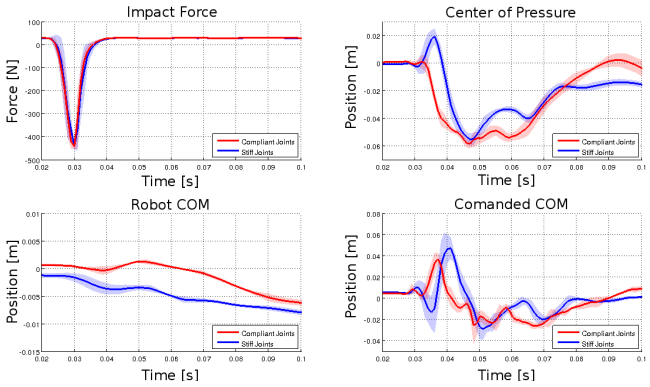


Fig. 7. System response in the first 0.1 seconds after impact (on the body).

robot above and below the actuated joint respectively. Each experiment is performed first with the robot ankles equipped with the elastic elements and then with the stiff connector. It must be noticed that the employment of the elastic elements increases the overall compliance of the system during the balancing task, which is determined, in the stiff case, only by the controller gains $k_p$, $k_d$ in (1). Thus, in order to obtain a fair comparison, the gains of the balance algorithm are adjusted to obtain the same equivalent stiffness at the ankle level (Fig. 5). Additionally, to simplify the analysis of the system, the controller was activated only in the robot's sagital plane, i.e. for the ankle forward/backward motion (one degree of freedom), and turned off the body attitude controller [12] which is normally used to minimize the spin angular momentum with the counter-rotation of the torso with respect to the ankle's. For each experiment, the impact force, the COP, the desired and estimated COM position are recorded. The time period of the control loop is $1ms$.

### A. Impact on the robot's body

In this experiment the robot, which is balancing on a static flat surface, is directly hit by a mass at the height of the COM, in the lower part of the torso. This mass is constituted by a standard bowling ball (6.35Kg), attached to the ceiling with a rope, about $2.20m$ long. The ball is released from a distance of about $1.0m$ from the robot. A force sensor has been also placed at the point of impact, in order to obtain a direct measurement of the impact force as shown in Fig. 6. After hitting the robot ten times releasing the ball always from the same distance with compliant and stiff ankles, Fig. 7 and Fig. 8 are obtained displaying mean and standard deviation values of the impact force, center of pressure, robot's COM and commanded COM for all trials with two different time scales ($0.1s$ and $2s$ seconds respectively, namely micro and macro scales from this point onwards). Since we are mainly interested on the collission instant and the transient response of the system, larger time scales are not explored. The distance from which the ball was thrown generated the maximum force possible before the robot tipped over. The high repeatability of the experiment can be appreciated as well as the expected backwards motion of the center of pressure after the impact which happens much faster than the COM motion. At the macro time scale the controller exhibits a $60ms$ delay from the impact instant in both stiff and compliant cases, **while the computed center of pressure presents a smoother behaviour in the compliant case right after the impact**.

### B. Impact on the platform

Since apart from the COP behaviour no significant difference in the overall system behaviour is noticed with and without physical compliance at the ankle level, a different experimental setup is used. This time the robot is balancing on top of a wheeled platform, which is hit by the same mass. The force sensor is now located on the mobile platform, in order to measure the impact force. The ball is then thrown with an angle such that the transmitted force is as close as possible to $400N$ as in the former experiment. This is illustrated in Fig. 9. Although the torque generated at the ankle might differ in both cases, what is important here is where the disturbance is applied.

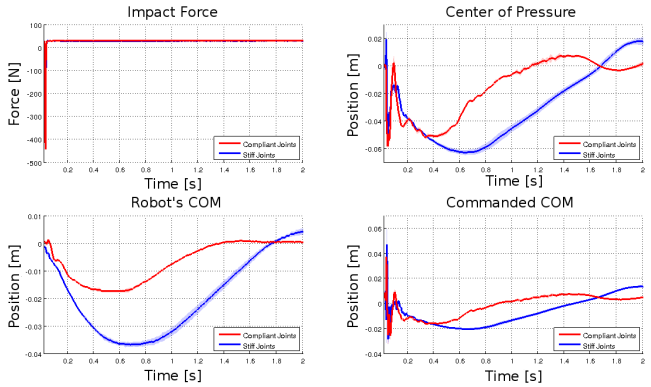


Fig. 8. System response in the first 2 seconds after the impact (on the body).

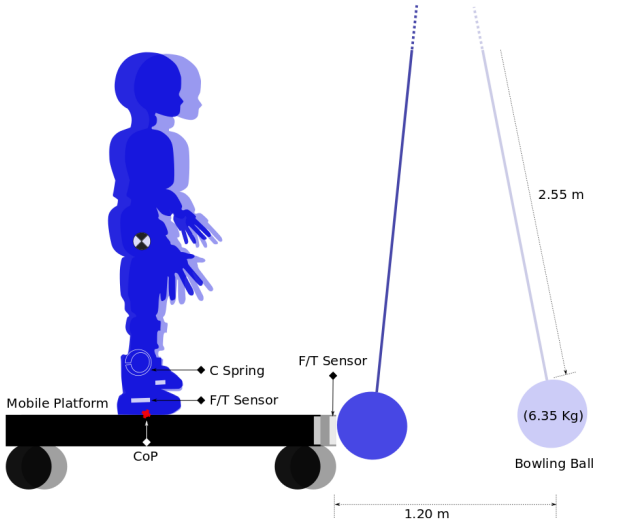


Fig. 9. A sketch of the second experimental setup: impact on the platform.

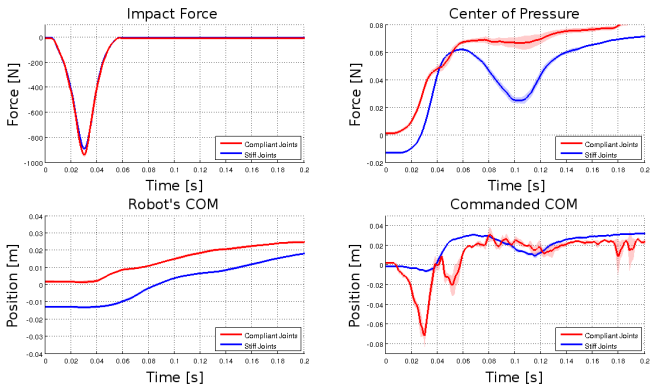


Fig. 10. System response in the first 0.2 seconds after the impact (on the platform).

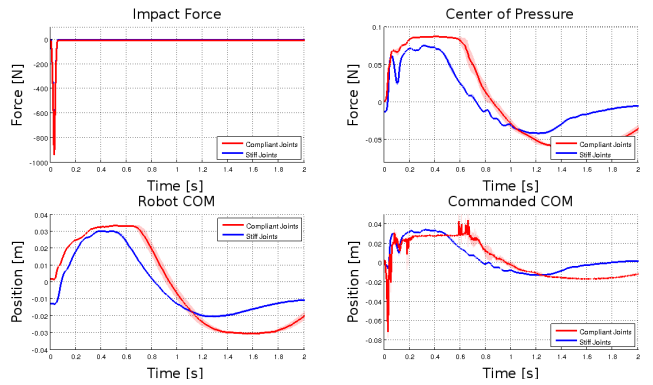


Fig. 11. System response in the first 2 seconds after impact (on the platform).

Similarly ten trials are done with both stiff and compliant ankles with high repeatability and small variance as it can be seen in Fig. 10 and Fig. 11. When hitting the robot's COM, the linear momentum is instantaneously transmitted to the top part of the robot, which is not compliant as the ankle, probably masking up a more significant effect of the springs. For this reason, in this new setup the system is perturbed first at the ankle level by a quick backward motion of the supporting mobile platform. In this way, the linear momentum passes directly through the ankles and **once more a filtering effect on the center of pressure can be observed also indicating a slower acceleration of the robot's center of mass**. The effect is more noticeable at both micro and macro time scales.

## V. Acknowledgments

This work is supported by the FP7 European projects AMARSi (FP7-ICT-2010-03 number 248311) and CoDyCo, (FP7-ICT-2011-9 number 600716).

## VI. Conclusions

In this paper we have shown the benefits of series elastic actuators in balancing tasks. The assumptions of the paper were to apply the very same perturbation on a standing robot, first equipped with series elastic actuators and then locking the transmission, as to have compliant and stiff ankles in the same setup. In order to perform a significant comparison experimental conditions were controlled in several ways. On one hand, perturbations were repeated several times, averaged over trials and standard deviations maintained relatively low for sake of repetitiveness. On the other hand, the performance of the balance controller was tried to keep as similar as possible in each experiment. At the low level, actuators were controlled with a simple position controller whose gains were kept constant for both the rigid and elastic condition. At the high level, the center of pressure was controlled with a simple feedback strategy whose proportional gain was adapted to maintain constant the overall system stiffness, compensating for the transmission elasticity. Thanks to these conditions, differences in results for the two joint setups can be attributed to the type of transmission used, showing a more stable balance recovery with SEA during the settling time which can be explained by the low pass filter effect of the series elastic actuators on the zero moment point dynamics.

## References

[1] Rodney A. Brooks, Cinthia Breazeal, M. Marjanovic, Brian Scassellati, and Matthew Williamson. *The Cog*

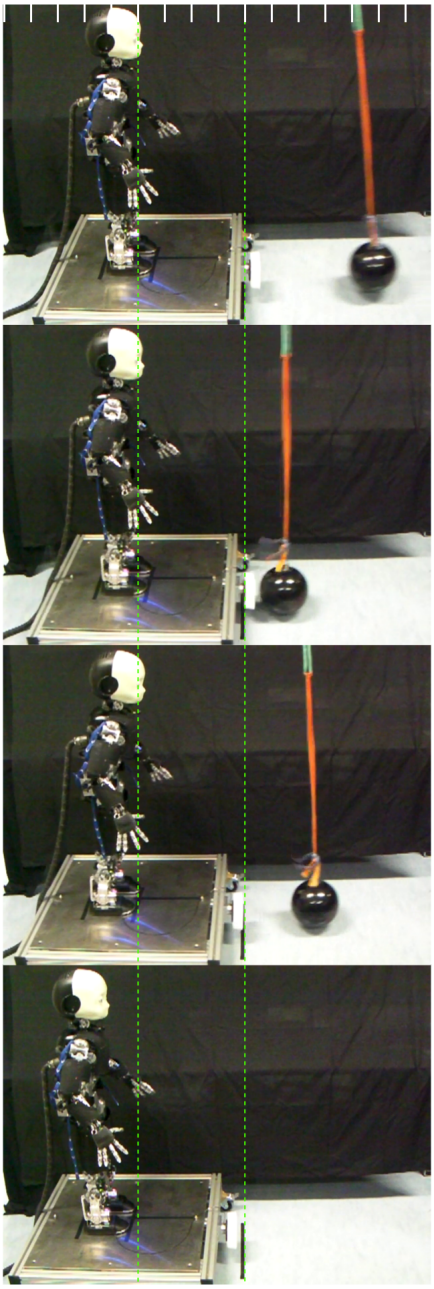

Fig. 12. A sequence of pictures showing the system balancing reaction after an impact on the support platform. Dotted green lines aid visualizing the initial and final position of the platform and how the robot moves from its initial equilibrium posture.


*project: Building a humanoid robot*, page 5287. Springer, New York, 1999. Lecture Notes in Artificial Intelligence 1562.

[2] Aaron Edsinger-Gonzales and Jeff Weber. Domo: a force sensing humanoid robot for manipulation research. *International Journal of Humanoid Robotics*, 1:279–291, 2004.

[3] D. Gouaillier, V. Hugel, P. Blazevic, C. Kilner, J. Monceaux, P. Lafourcade, B. Marnier, J. Serre, and B. Maisonnier. Mechatronic design of NAO humanoid. In *Proc. IEEE Int. Conf. on Robotics and Automation (ICRA)*, pages 2124–2129, 2009.

[4] M. Grebenstein, A. Albu-Schaffer, T. Bahls, M. Chalon, O. Eiberger, W. Friedl, R. Gruber, S. Haddadin, U. Hagn, R. Haslinger, H. Hoppner, S. Jorg, M. Nickl, A. Nothhelfer, F. Petit, J. Reill, N. Seitz, T. Wimbock, S. Wolf, T. Wusthoff, and G. Hirzinger. The DLR hand arm system. In *Proc. IEEE Int. Conf. on Robotics and Automation (ICRA)*, pages 3175 –3182, may 2011. doi: 10.1109/ICRA.2011.5980371.

[5] Masato Hirose and Kenichi Ogawa. Honda humanoid robots development. *Philosophical Transactions of the Royal Society*, 365(1850):11–19, 2007. doi: 10.1098/rsta.2006.1917.

[6] Sang Ho Hyon and Gordon Cheng. Gravity compensation and full-body balancing for humanoid robots. In *IEEE-RAS International Conference on Humanoid Robots*, pages 214–221, December 2006.

[7] Chris A. Ihrke, Adam H. Parsons, Joshua S. Mehling, and Bryan Kristian Griffith. Planar torsion spring. Patent, Jun 2010.

[8] Tatsuzo Ishida, Yoshihiro Kuroki, and Jinichi Yamaguchi. Mechanical system of a small biped entertainment robot. In *Proc. IEEE/RSJ Int. Conf. on Intelligent Robots and Systems (IROS)*, pages 1129–1134, October 2003.

[9] K. Kaneko, F. Kanehiro, M. Morisawa, K. Miura, S. Nakaoka, and S. Kajita. Cybernetic human HRP-4C. In *Proc. IEEE/RAS Int. Conf. on Humanoid Robots (HUMANOIDS)*, pages 7–14, 7-10 2009. doi: 10.1109/ICHR.2009.5379537.

[10] T. Lens, J. Kunz, O. Stryk, C. Trommer, and A. Karguth. BioRob-arm: a quickly deployable and intrinsically safe, light-weight robot arm for service robotics applications. In *6th German Conference on Robotics (ROBOTIK)*. VDE, 2010.

[11] Zhibin Li, Nikolaos Tsagarakis, and Darwin G. Caldwell. A passivity based admittance control for stabilizing the compliant humanoid COMAN. In *IEEE-RAS International Conference on Humanoid Robots*, pages 44–49, Osaka, Japan, Nov. 29th - Dec. 1st 2012.

[12] Zhibin Li, Bram Vanderborght, Nikos G. Tsagarakis, Luca Colasanto, and Darwin G. Caldwell. Stabilization for the Compliant Humanoid Robot COMAN Exploiting Intrinsic and Controlled Compliance. In *IEEE International Conference on Robotics and Automation*, Minnesota, USA, May 2012.

[13] C. Ott, C. Baumgartner, J. Mayr, M. Fuchs, R. Burger, D. Lee, O. Eiberger, A. Albu-Schaffer, M. Grebenstein, and G. Hirzinger. Development of a biped robot with torque controlled joints. In *10th IEEE-RAS International Conference on Humanoid Robots*, pages 167–173, 2010.

[14] C. Ott, M.A. Roa, and G. Hirzinger. Posture and balance control for biped robots based on contact force optimization. In *11th IEEE-RAS International Conference on Humanoid Robots (Humanoids)*, pages 26–33, Bled, Slovenia, 2011.

[15] I.W. Park, J.Y. Kim, J. Lee, and J.H. Oh. Mechanical design of the humanoid robot platform HUBO. *Advanced Robotics*, 21(11):1305–1322, 2007.

[16] Alberto Parmiggiani, Marco Maggiali, Lorenzo Natale, Francesco Nori, Alexander Schmitz, Nikos Tsagarakis, Joseé Santos Viktor, Francesco Becchi, Giulio Sandini, and Giorgio Metta. The design of the iCub humanoid robot. *International Journal of Humanoid Robotics*, 2012. accepted for publication.

[17] G.A. Pratt and M.M. Williamson. Series elastic actuators. In *Proc. IEEE/RSJ Int. Conf. on Intelligent Robots and Systems (IROS)*, pages 399–406, 1995.

[18] J. Pratt and B. Kruppb. Design of a bipedal walking robot. In *Proc. of SPIE*, volume 6962, pages 69621F1–69621F13, 2008.

[19] B.J. Stephens and C.G. Atkeson. Dynamic balance force control for compliant humanoid robots. In *IEEE/RSJ International Conference on Intelligent Robots and Systems*, pages 1248–1255. IEEE, 2010.

[20] Stephen P. Timoshenko and J.N. Goodier. *Theory of Elasticity*. McGraw-Hill, 1970.

[21] N.G. Tsagarakis, Matteo Laffranchi, Bram Vanderborght, and D.G. Caldwell. A compact soft actuator unit for small scale human friendly robots. In *Proc. IEEE Int. Conf. on Robotics and Automation (ICRA)*, pages 4356 –4362, may 2009. doi: 10.1109/ROBOT.2009.5152496.

[22] N.G. Tsagarakis, Zhibin Li, J. Saglia, and D.G. Caldwell. The design of the lower body of the compliant humanoid robot cCub. In *Proc. IEEE Int. Conf. on Robotics and Automation (ICRA)*, pages 2035 –2040, may 2011. doi: 10.1109/ICRA.2011.5980130.

[23] S. Wolf, O. Eiberger, and G. Hirzinger. The DLR FSJ: Energy based design of a variable stiffness joint. In *Proc. IEEE Int. Conf. on Robotics and Automation (ICRA)*, pages 5082 –5089, may 2011. doi: 10.1109/ICRA.2011.5980303.